Mechanism of $Ir(ppy)_2(N^N)^+$ (N^N = 2-Phenyl-1*H*-imidazo[4,5-*f*][1,10]phenanthroline) Sensor for F^-, CF_3COOH, and CH_3COO^-: Density Functional Theory and Time-Dependent Density Functional Theory Studies

Tao Liu,[†] Hong-Xing Zhang,*[,†] Xin Zhou,[†] Qing-Chuan Zheng,[†] Bao-Hui Xia,[‡] and Qing-Jiang Pan[§]

State Key Laboratory of Theoretical and Computational Chemistry, Institute of Theoretical Chemistry, Jilin University, Changchun 130023, People's Republic of China, College of Chemistry, Jilin University, Changchun 130023, People's Republic of China, and Laboratory of Physical Chemistry, School of Chemistry and Materials Science, Heilongjiang University, Harbin 150080, People's Republic of China

Received: May 4, 2008; Revised Manuscript Received: June 16, 2008

The geometries, electronic structures, and spectroscopic properties of $Ir(ppy)_2(N^N)^+$ (**1**) (N^N = 2-phenyl-1*H*-imidazo[4,5-*f*][1,10]phenanthroline, ppy = 2-phenylpyridine), $Ir(ppy)_2(N^N)^+ \cdot F^-$ (**2**), $Ir(ppy)_2(N^N)^+ \cdot CF_3COOH$ (**3/3a**), and $Ir(ppy)_2(N^N)^+ \cdot CH_3COO^-$ (**4**) were investigated theoretically. The ground and the excited state geometries of **1**−**4** were optimized at the B3LYP/LANL2DZ and UB3LYP/LANL2DZ levels, respectively. The optimized geometries agree well with the corresponding experimental results. The HOMOs of **1**−**4** and **3a** are composed of π(ppy) and d(Ir), and the LUMOs of **1**, **2**, **3a**, and **4** are contributed by π^*(N^N), whereas the LUMO of **3** is composed of π^*(N^N) and $\pi^*(CF_3COOH)$. Under the time-dependent density functional theory level with polarized continuum model model, the absorption and phosphorescence in CH_2Cl_2 media were calculated on the basis of the optimized ground and excited state geometries, respectively. The lowest-lying absorptions of **1** (412 nm) and **3/3a** (409/419 nm) have MLCT/LLCT transition characters, and those of **2** (448 nm) and **4** (427 nm) are contributed by ILCT character. The calculated lowest-energy triplet excited states responsible for phosphorescence of **1** (519 nm) and **3/3a** (661/702 nm) have mixing ^{3}MLCT/^{3}LLCT/^{3}ILCT characters, but those of **2** and **4** only have ^{3}ILCT but without ^{3}MLCT character, which is the reason for the no-emissive character of **2** and **4**. Moreover, the phosphorescence character of **3** is hardly changed by different addition sites of CF_3COOH group (**3a**). The calculated results also showed that complex **1** is more suitable for an F^- sensor than for CF_3COOH and CH_3COO^- sensors.

Introduction

The photophysical and photochemical properties of phosphorescent transition-metal complexes such as Ru(II), Os(II), Re(I), Rh(III), Pt(II) and Ir(III) species with d^6 and d^8 configuration have been thoroughly investigated over the past two decades.[1] The strong spin−orbital coupling of heavy transition metals leads to an efficient mixing of singlet and triplet excited states, as well as the enhancement of the intensity of triplet metal-to-ligand charge transfer (^{3}MLCT) excited state by effectively borrowing that of the singlet MLCT excited state. Thus, they have been successfully applied in various potential fields including organic light emitting devices (OLEDs),[2] biological labeling reagents,[3] and catalyst.[4]

In the past few decades, the development of a colorimetric sensor has been particularly challenging because the visual detection can give immediate qualitative information and is becoming increasingly appreciated in terms of quantitative analysis. The sensor based on the fluorescent organic fluorophoric units has attracted much attention due to the high sensitivity and selectivity of metal-ion sensing based on fluorescence signal.[5]

CHART 1: Structures of 1−4 and 3a

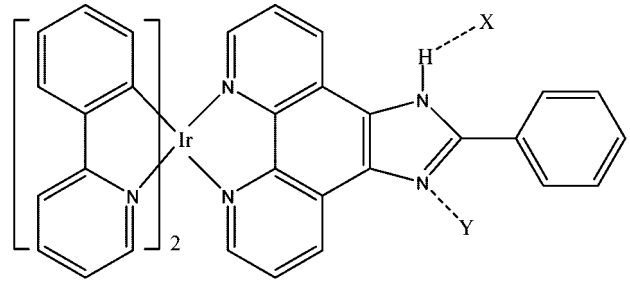

X = None (1), F- (2), CF3COOH (3), CH3COO- (4); Y = CF3COOH (3a)

Recently, the use of phosphorescent transition-metal complexes as chemosensors has attracted considerable interest,[6] because of advantageous photophysical properties of transition-metal complexes such as relatively long lifetimes and high stability compared with those of pure organic luminophores.[7] Furthermore, phosphorescence is indeed one of the most sensitive analytical techniques because it is nondestructive, relatively inexpensive, and easy to use and represents a sustainable technology.[8] Many phosphorescent transition-metal complexes with d^6 and d^8 electron configurations including Pt(II), Re(I), Ru(II) complexes have been applied as chemosensors for pH, oxygen, metal ions (Mg^+, Ca^+), and nonmetal ions (F^-, CH_3COO^-, $H_2PO_4^-$) by many researchers.[9–14]

* To whom correspondence should be addressed. E-mail: zhanghx@mail.jlu.edu.cn.
† Institute of Theoretical Chemistry, Jilin University.
‡ College of Chemistry, Jilin University.
§ Heilongjiang University.

10.1021/jp803996y CCC: $40.75
Published on Web 08/14/2008

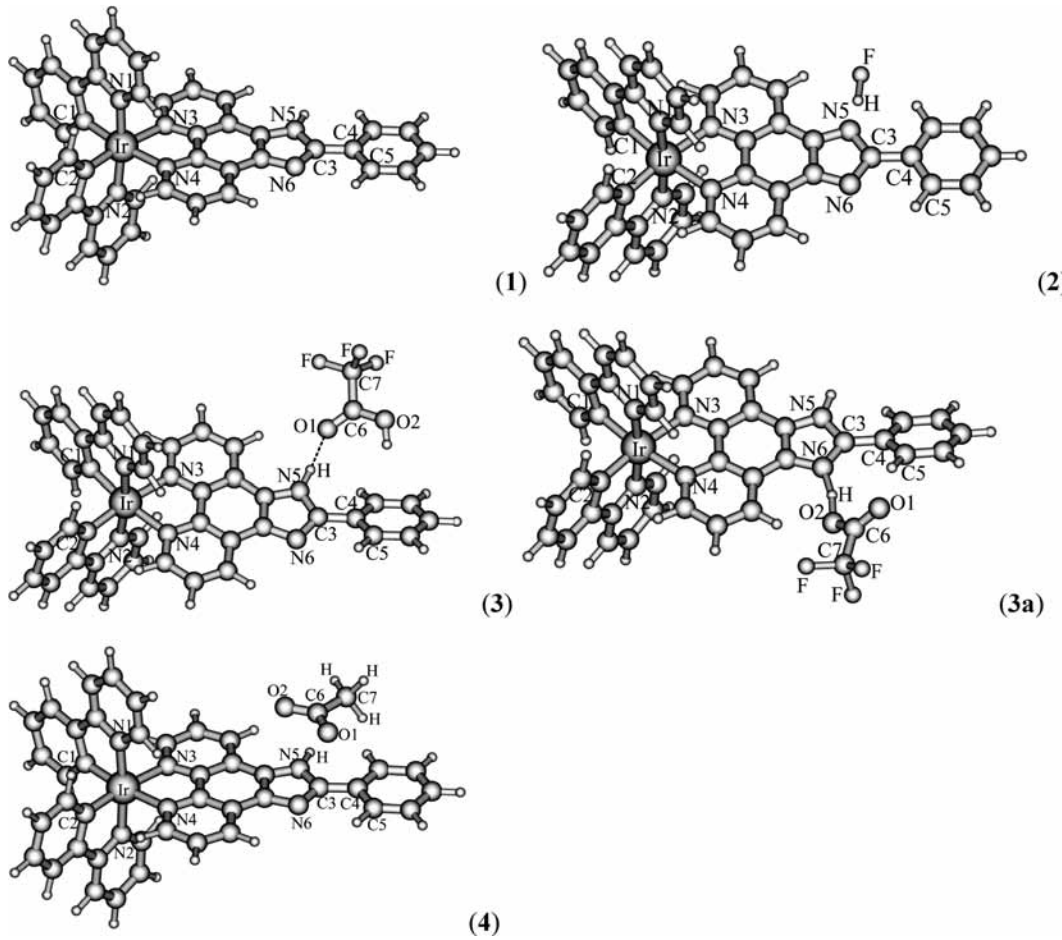

Figure 1. Optimized ground state geometries of **1**−**4** and **3a** optimized at the B3LYP/LANL2DZ level.

Since it was reported that OLEDs prepared with Ir(ppy)$_3$ (ppy$^-$ = 2-phenylpyridine) have efficiencies greater than 80%, Ir(III) complexes have attracted much more attention.[15–18] As one of the best families of phosphorescent dyes, iridium(III) complexes have been used as chemosensors for oxygen,[8,19,13] homocysteine,[20] ions such as Hg^{2+},[21] Ag^+,[22] Cl^-,[23] and biomolecules.[24] Recently, a series of cationic iridium(III) with different phenanthroline derivatives ligands were synthesized by Li and Huang, and the photophysical and electrochemical properties were also investigated.[25] They found that the emission of the complexes with the 1*H*-imidazo[4,5-*f*][1,10]phenanthroline ligand can be red-shifted by addition of CF_3COOH and quenched by addition of F$^-$, CH_3COO^-, and $H_2PO_4^-$ groups, which can be observed by the naked eyes, moreover, the binding constants of these iridium complexes for F$^-$, CH_3COO^-, and $H_2PO_4^-$ confirm that the reaction between the NH bond of the imidazolyl group and CH_3COO^-, $H_2PO_4^-$ is a hydrogen-bonding effect, but a deprotonation process between F$^-$ and imidazolyl group. Furthermore, they carried out density functional theory (DFT) calculation to understand the properties of the highest occupied molecular orbital (HOMO) and lowest unoccupied molecular orbital (LUMO). But, to the best of our knowledge, there is no theoretical calculation on the absorption and phosphorescence mechanism of the Ir(III) complexes sensors from electronic structure point of view.

Using above background, we carried out the present DFT calculation work on Ir(ppy)$_2$(N^N)$^+$ (**1**) (N^N = 2-phenyl-1*H*-imidazo[4,5-*f*][1,10]phenanthroline, ppy = 2-phenylpyridine), Ir(ppy)$_2$(N^N)$^+\cdot$F$^-$ (**2**), Ir(ppy)$_2$(N^N)$^+\cdot CF_3COOH$ (**3** and **3a**), and Ir(ppy)$_2$(N^N)$^+\cdot CH_3COO^-$ (**4**) (see Chart 1), aimed at providing an in-depth theoretical understanding of the ground and the excited state geometries, electronic structures, absorption and emission properties of **1**−**4** and **3a**. Most importantly, the different interactions between Ir(ppy)$_2$(N^N)$^+$ and F$^-$, CF_3COOH, and CH_3COO^- groups as well as the reason for the phosphorescence quenching upon addition of F$^-$ and CH_3COO^- were revealed. In addition, the two different adsorption sites (addition on N5−H (**3**) and N6 (**3a**) sites) of

TABLE 1: Main Optimized Geometry Parameters of 1−4 in the Ground and the Lowest-Lying Triplet Excited State, Together with the Experimental Values of 1

	1		**2**		**3**		**4**		
parameters	X^1A	A^3A	X^1A	X^3A	A^1A	A^3A	X^1A	X^3A	**1** expt[a]
Ir−N1	2.075	2.073	2.069	2.065	2.073	2.072	2.069	2.064	2.037
Ir−N2	2.074	2.070	2.069	2.065	2.074	2.071	2.069	2.065	2.042
Ir−N3	2.175	2.167	2.171	2.161	2.177	2.164	2.171	2.162	2.144
Ir−N4	2.173	2.164	2.171	2.159	2.177	2.168	2.169	2.154	2.139
Ir−C1	2.032	2.011	2.032	2.034	2.032	2.009	2.032	2.035	2.018
Ir−C2	2.031	2.011	2.032	2.033	2.031	2.009	2.032	2.034	2.010
F−H			1.102	1.048					
H−O1					1.830	1.881	1.459	1.079	
N5−H	1.010	1.010	1.322	1.400	1.021	1.019	1.104	1.508	
C−Ir−C	89.9	95.3	89.7	90.0	90.1	95.9	89.6	89.8	88.6
C1−Ir−N1	80.3	81.1	80.3	80.3	80.3	81.1	80.3	80.3	80.5
N1−Ir−N2	173.5	176.9	174.4	174.6	173.4	177.1	174.6	174.9	170.8
N3−Ir−N4	77.2	77.4	77.5	77.6	77.1	77.3	77.3	77.4	77.1
N6−C3−C4	125.4	125.4	123.8	123.3	125.8	125.5	122.8	120.0	
F−H−N5			171.8	178.1					
N5−H−O1					168.5	165.6	172.5	165.1	
N6−C3−C4-C5	0.3	0.5	0.5	0.2	27.5	25.6	0.5	0.6	
H−O1−C6-O2					17.2	19.3	0.8	0.2	
N5−H−O1-C6					57.4	48.2	176.2	178.7	

[a] ref.[25]

TABLE 2: Molecular Orbital Compositions (%) in the Ground State of 1 at the B3LYP Level

orbital	energy (eV)	Ir	N^N	C^N	main bond type	Ir components
L+4	−1.99		67.1	31.6	π^*(N^N) + π^*(C^N)	
L+3	−2.02		29.8	66.8	π^*(N^N) + π^*(C^N)	
L+1	−2.51		97.1		π^*(N^N)	
L	−2.83		94.3		π^*(N^N)	
			HOMO−LUMO Energy Gap			
H	−5.86	44.1		51.2	d_{xz} + d_{z^2} + $d_{x^2-y^2}$ + π(C^N)	19.5 d_{xz} 15.7 d_{z^2} 8.7 $d_{x^2-y^2}$
H−1	−6.43	20.4	60.2	19.4	d_{xy} + d_{yz}+ π(N^N) + π(C^N)	9.5 d_{xy} 10.8 d_{yz}
H−2	−6.53		30.1	67.7	π(N^N) + π(C^N)	
H−3	−6.61	57.6		37.6	d_{xz} + d_{z^2} + π(C^N)	31.9 d_{xz} 22.9 d_{z^2}
H−7	−7.43		99.5		π(N^N)	
H−8	−7.59		97.5		π(N^N)	

TABLE 3: Molecular Orbital Compositions (%) in the Ground State of 2 at B3LYP Level

orbital	energy (eV)	Ir	N^N	C^N	main bond type	Ir components
L+6	−1.23			96.8	π^*(C^N)	
L+5	−1.24		51.0	47.5	π^*(N^N) +π^*(C^N)	
L+4	−1.47		49.0	50.2	π^*(N^N) +π^*(C^N)	
L+3	−1.76		18.5	78.6	π^*(N^N) + π^*(C^N)	
L+1	−1.87		78.4	19.6	π^*(N^N) + π^*(C^N)	
L	−2.34		94.1		π^*(N^N)	
			HOMO−LUMO Energy Gap			
H	−5.61	45.3		50.1	d_{xz} + d_{z^2} + $d_{x^2-y^2}$ + π(C^N)	15.0 d_{xz} 18.7 d_{z^2} 11.4 $d_{x^2-y^2}$
H−1	−5.67		97.0		π(N^N)	
H−2	−6.28	22.8		71.6	d_{xy} + d_{yz} + π(C^N)	12.0 d_{xy} 10.6 d_{yz}
H−3	−6.32	62.8		30.8	d_{xz} + d_{z^2} + π(C^N)	37.9 d_{xz} 24.2 d_{z^2}
H−5	−6.62		15.1	72.7	π(N^N) + π(C^N)	
H−6	−6.73		70.7	24.8	π(N^N) + π(C^N)	
H−7	−6.75		21.6	67.3	π(N^N) +π(C^N)	

TABLE 4: Molecular Orbital Compositions (%) in the Ground State of 3 at B3LYP Level

orbital	energy (eV)	Ir	N^N	C^N	CF_3COOH	main bond type	Ir components
L+2	−2.51		95.7			π^*(N^N)	
L+1	−2.84		74.8		20.8	π^*(N^N) + π^*(CF_3COOH)	
L	−2.88		21.8		77.1	π^*(N^N) + π^*(CF_3COOH)	
				HOMO−LUMO Energy Gap			
H	−5.86	44.0		51.2		d(Ir) + π(C^N)	5.6 d_{xz} 7.7 d_{yz} 18.6 d_{z^2} 10.5 $d_{x^2-y^2}$
H−1	−6.48	26.0	18.1	55.8		d(Ir) + π(N^N) + π(C^N)	18.1 d_{xy}
H−2	−6.61	23.6	38.8	37.6		d(Ir) + π(N^N) + π(C^N)	8.5 d_{xz} 5.4 d_{z^2} 6.1 $d_{x^2-y^2}$
H−3	−6.62	44.8	18.0	37.2		d(Ir) + π(N^N) + π(C^N)	17.9 d_{xz} 5.4 d_{yz} 9.6 d_{z^2} 5.8 $d_{x^2-y^2}$ 5.9 d_{xy}
H−6	−6.98	25.0	12.2	62.8		d(Ir) + π(N^N) + π(C^N)	17.6 d_{xy} 4.7 d_{yz}
H−7	−7.59		97.5			π(N^N)	

TABLE 5: Molecular Orbital Compositions (%) in the Ground State of 4 at B3LYP Level

orbital	energy (eV)	Ir	N^N	C^N	main bond type	Ir components
L+6	−1.24			97.0	π^*(C^N)	
L+4	−1.53		68.3	31.1	π^*(N^N) + π^*(C^N)	
L+3	−1.77		9.3	87.2	π^*(N^N) + π^*(C^N)	
L+2	−1.86			93.9	π^*(C^N)	
L+1	−1.93		88.8	9.8	π^*(N^N) + π^*(C^N)	
L	−2.37		94.2		π^*(N^N)	
			HOMO−LUMO Energy Gap			
H	−5.62	45.2		50.1	d(Ir) + π(C^N)	29.1 d_{z^2} 10.4 $d_{x^2-y^2}$
H-1	−5.84		94.7		π(N^N)	
H-2	−6.29	20.2		73.3	d(Ir) + π(C^N)	16.7 d_{xy}
H-5	−6.48	44.7	11.8	43.5	d(Ir) + π(N^N) + π(C^N)	42.3 d_{xy}
H-7	−6.75	11.9		83.3	d(Ir) + π(C^N)	8.8 d_{xy}

CF_3COOH group connected to the N^N ligand were considered in our calculation.

Computational Details

The ground and the excited state geometries of **1**−**4** and **3a** were fully optimized by the DFT[26] method with Becke's three parameter functional and the Lee−Yang−Parr functional[27] (B3LYP) and unrestricted B3LYP (UB3LYP) approaches, respectively, without symmetry restriction. Spin contamination due to the admixture of excitations of higher multiplicity is rather small: the expectation values of spin operator $\langle S^2 \rangle$ are about 2.02 for triplet states. On the basis of the optimized ground

TABLE 6: Calculated HOMO and LUMO Energy Levels of 1−4 in CH_2Cl_2 Media and Gas Phase

	1			**2**		**3**		**4**	
	gas	CH_2Cl_2	gas[a]	gas	CH_2Cl_2	gas	CH_2Cl_2	gas	CH_2Cl_2
LUMO	−5.04	−2.83	−4.84	−2.35	−2.34	−4.96	−2.88	−2.44	−2.37
HOMO	−7.76	−5.86	−7.71	−5.25	−5.61	−7.72	−5.86	−5.30	−5.62

[a] ref.[25]

TABLE 7: The Absorptions of 1−4 in CH_2Cl_2 Calculated Using the TDDFT Method, Together with the Experimental Values of 1

	transition	config (CI coeff)	*E*/nm (eV)	oscillator	assignment	λ_{exp}/nm (eV)[a]
1	$X^1A \rightarrow A^1A$	H−1 → L (0.57)	412 (3.01)	0.15	MLCT/LLCT	416 (2.98)
		H−3 → L (0.32)			MLCT/LLCT	
	$X^1A \rightarrow B^1A$	H−2 → L+1 (0.58)	351 (3.54)	0.09	LLCT/ILCT	348 (3.56)
	$X^1A \rightarrow C^1A$	H−2 → L+4 (0.52)	304 (4.08)	0.28	LLCT/ILCT	299 (4.15)
	$X^1A \rightarrow D^1A$	H−7 → L+1 (0.40)	280 (4.43)	0.28	ILCT	279 (4.44)
		H−8 → L+1 (0.40)			ILCT	
2	$X^1A \rightarrow A^1A$	H−1 → L (0.68)	448 (2.77)	0.12	ILCT	
	$X^1A \rightarrow B^1A$	H−2 → L (0.63)	371 (3.34)	0.09	MLCT/LLCT	
	$X^1A \rightarrow C^1A$	H−1 → L+4 (0.66)	330 (3.75)	0.52	LLCT/ILCT	
	$X^1A \rightarrow D^1A$	H−6→ L+1 (0.42)	285 (4.35)	0.27	ILCT	
		H−5→ L+3 (0.26)			ILCT	
		H−3→ L+6 (0.24)			MLCT/ILCT	
		H−7→ L+1 (0.24)			LLCT	
	$X^1A \rightarrow E^1A$	H−3→ L+5 (0.42)	273 (4.54)	0.27	MLCT/ILCT	
		H-2→ L+6 (0.27)			MLCT/ILCT	
		H−7→ L+3 (0.23)			ILCT	
3	$X^1A \rightarrow A^1B$	H−1 → L+1 (0.53)	409 (3.03)	0.15	MLCT/LLCT	
	$X^1A \rightarrow B^1B$	H−3 → L+2 (0.44)	353 (3.51)	0.05	MLCT/LLCT	
		H−2 → L+2 (0.35)			MLCT/LLCT	
	$X^1A \rightarrow C^1B$	H−6 → L+1 (0.51)	344 (3.60)	0.06	MLCT/LLCT	
	$X^1A \rightarrow D^1B$	H−7 → L+2 (0.52)	277 (4.47)	0.36	ILCT	
4	$X^1A \rightarrow A^1B$	H−1 → L (0.68)	427 (2.91)	0.15	ILCT	
	$X^1A \rightarrow B^1B$	H−1 → L+1 (0.63)	364 (3.40)	0.06	ILCT	
	$X^1A \rightarrow C^1B$	H−-1 → L+4 (0.48)	323 (3.84)	0.44	ILCT/LLCT	
		H−7 → L (0.36)			LLCT/MLCT	
		H−2 → L+2 (0.26)			MLCT/ILCT	
	$X^1A \rightarrow D^1B$	H−2 → L+6 (0.44)	273 (4.53)	0.41	MLCT/ILCT	
		H−7 → L+3 (0.25)			MLCT/ILCT	
		H−5 → L+6 (0.21)			MLCT/ILCT/LLCT	

[a] reference 25.

and the excited state geometries, the molecular orbital compositions, charge population, absorption and emission spectra in CH_2Cl_2 media were calculated by time-dependent DFT[28] (TD-DFT) associated with the polarized continuum model (PCM).[29] This kind of theoretical approach and calculation level has been proven to be reliable for transition-metal complex systems by previous works.[30]

In the calculations, the quasi-relativistic pseudopotentials of Ir atoms proposed by Hay and Wadt[31] with 17 valence electrons were employed, the ground state geometry and the absorption spectra of **1** were calculated with two basis sets: BS(I), LANL2DZ for Ir and 6-31G* for other atoms; BS(II), LANL2DZ basis sets for all atoms. The calculated results showed that the geometry obtained by BS(II) is more consistent with the experimental values than that obtained by BS(I), and the absorption spectra are hardly changed by using different basis sets (BS(I) and BS(II)). Thus we adopted BS(II) for the following calculations, moreover, the present calculation level was enough to obtain satisfied results. The basis sets were described as Ir (8s6p4d)/[3s3p2d], C, N, O and F (10s5p)/[3s2p], and H (4s)/[2s]. Thus, 501 basis functions and 332 electrons for **1**, 510 basis functions and 342 electrons for **2**, 566 basis functions and 388 electrons for **3/3a**, 543 basis functions and 364 electrons for **4**, were included in the calculations. All of the calculations were accomplished by using the Gaussian 03 software package[32] on an IBM server.

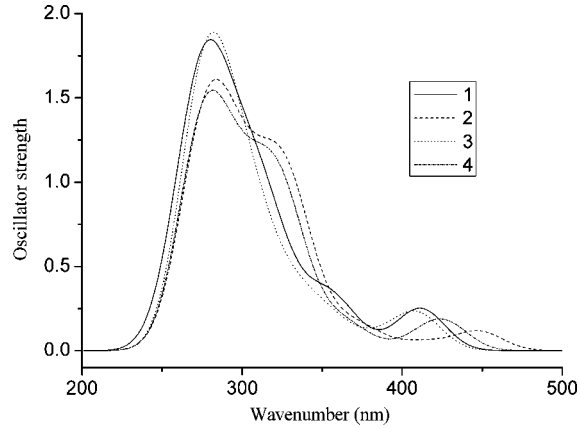

Figure 2. Simulated absorption spectra of **1**−**4** in CH_2Cl_2 media calculated at the TD-DFT/LANL2DZ level.

Results and Discussion

Ground and the Excited State Geometries. The main optimized ground state geometry parameters of **1**−**4** together with the X-ray crystal diffraction data of **1**[25] are given in Table 1, and the optimized geometries of **1**−**4** and **3a** are shown in Figure 1. Vibrational frequencies were calculated on the basis of the optimized geometries of **1**−**4** to verify that each of the

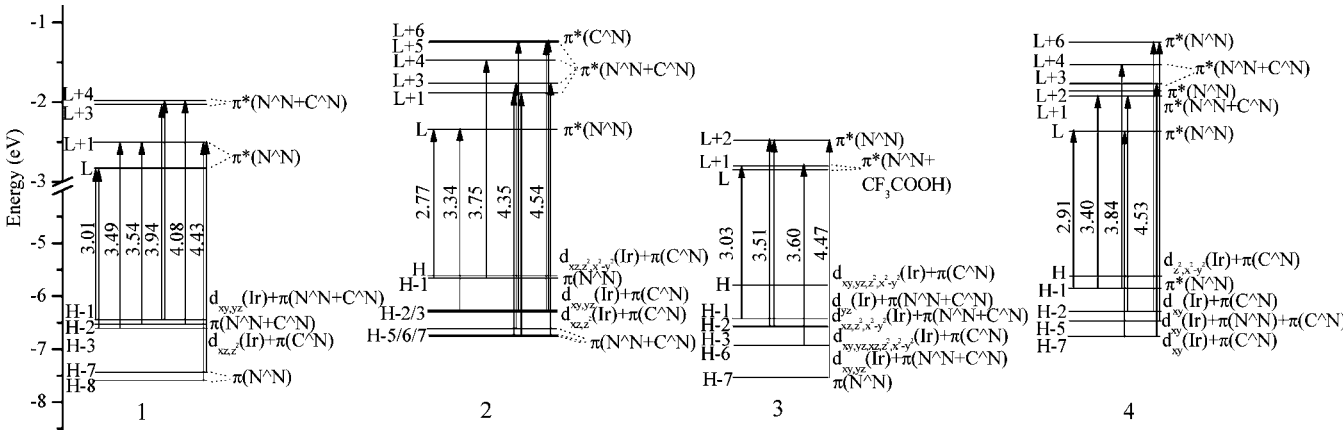

Figure 3. Diagrams of the molecular orbital related to the absorptions of **1**−**4**.

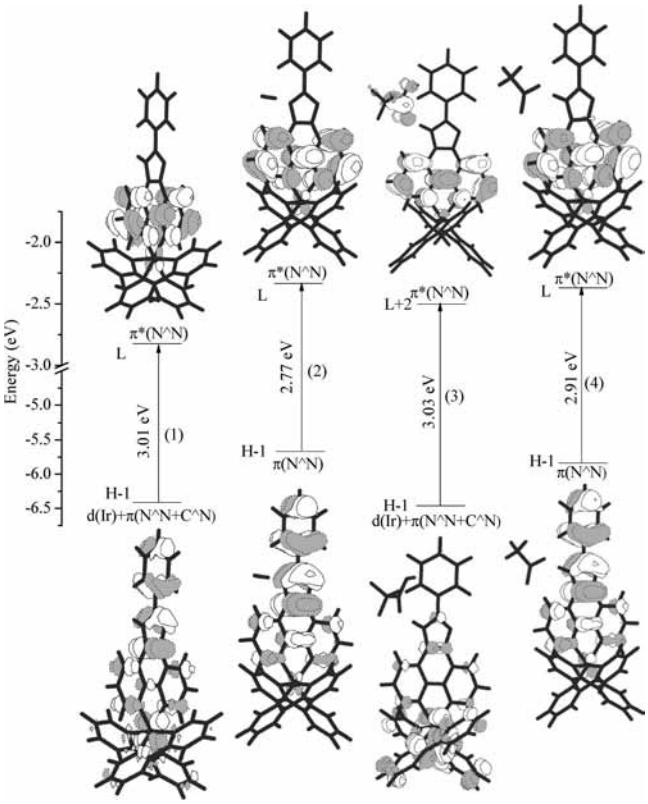

Figure 4. Transitions responsible for the lowest-lying absorption at 412, 448, 409, and 427 nm for **1**, **2**, **3**, and **4**, respectively.

geometries is a minimum (no minus frequency) on the potential energy surface.

With respect to **1**, the optimized bond lengths of Ir−N1 (2.075 Å), Ir−N2 (2.074 Å), Ir−N3 (2.175 Å), and Ir−N4 (2.173 Å) are consistent with the corresponding experimental values except a small deviation about 0.04 Å, the calculated bond lengths of Ir−C1 and Ir−C2 are overestimated by about 0.02 Å compared with the measured values.[25] The calculated bond angles of C1−Ir−C2, C1−Ir−N1, N3−Ir−N4, and N1−Ir−N2 are exactly consistent with the experimental values with a deviation about 1°.[25] The calculated bond angle of N1−Ir−N2 is 173.5°, indicating that N1, Ir, and N2 atoms are almost linear. The calculated dihedral angle of N6−C3−C4−C5 is 0.3° indicating that the phenyl ring and the phenanthroline are coplanar in the ground state. The discrepancy between the calculated and the measured geometry parameter is reasonable and acceptable because the environment of the complexes to stay on are different in the two case, in the latter one the molecule is in a tight crystal lattice[25] whereas in the former one the molecule is free.

Table 1 shows that the bond length N5−H of **1** is 1.010 Å. Compared with **1**, the N5−H bond of **2** (1.322 Å) and **4** (1.104 Å) are weakened by addition of F^- and CH_3COO^- groups, which also can be confirmed by the formation of the strong interaction between H and F^-, CH_3COO^-. With respect to **3**, the N5−H bond length is changed to 1.021 Å a little longer than that of **1**, which indicates that the N5−H is less weakened by addition of CF_3COOH than F^- and CH_3COO^-, which also can be confirmed by the formation of the weak hydrogen bond H−O1 (1.830 Å). The N5−H bond length results of **1**−**4** showed that the H (N5−H) of **2** breaks away from the N^N ligand at the most extent, whereas there is strong interactions between H (N5−H of **3** and **4**) and N^N ligand. Furthermore, on experiment, Li and Huang[25] reported that the reaction between the NH bond of the imidazolyl group and F^- is a deprotonation process, and there is strong interaction between the N^N ligand and CH_3COO^-. The N6−C3−C4 bond angles of **1**−**4** between 122.8° and 125.8° are hardly affected by addition of other groups. The dihedral angles N6−C3−C4−C5 of **1**, **2**, and **4** are less than 0.5°, which indicated that the phenyl ring is coplanar with phenanthroline. But the N6−C3−C4−C5 dihedral angle of **3** is 27.5°, which indicated that the phenyl ring is rotated by addition of CF_3COOH groups. N5−H−O1−C6 of **3** and **4** are 57.4° and 176.2°, indicating that the backbone of CH_3COO^- is coplanar with the N^N ligand, but CF_3COOH is out of the N^N plane. The geometry parameters of **3a** are similar to these of **3**.

The main geometry parameters of **1**−**4** in the A^3A excited states are also given in Table 1. The calculated results showed that the bond lengths Ir−N1/N2/N3/N4 of **1**−**4** are all strengthened by about 0.01 Å compared with the ground state values, indicating that the N^N ligand has a trend to get close to the Ir atom by excitation, and it is not affected by the addition of F^-, CF_3COOH, and CH_3COO^- groups. The Ir−C1/C2 of **2** and **4** are hardly changed by excitation, but Ir−C1/C2 of **1** and **3** are strengthened by about 0.02 Å relative to those in the ground state, which indicates that the C^N ligands of **1** and **3** have a trend to get close to the Ir atom. The N5−H bond of **1** and **3** are hardly changed, but those of **2** and **4** are greatly relaxed by ca. 0.078 and 0.404 Å, corresponding to the fact that the F−H and H−O1 bonds are shortened in the excited state, which indicates that the H atom has a trend to break away from phenanthroline and get close to F^- and CH_3COO^- groups in the excited state. The C−Ir−C bond angles of **1** and **3** are

TABLE 8: Calculated Phosphorescence of 1−4 with the TD-DFT Method, Together with the Experimental Value of 1

	transition	config (CI coeff)	*E*/nm (eV)	assignment	expt/nm (eV)[a]
1	$A^3A \rightarrow X^1A$	L → H−1 (0.68)	519 (2.39)	^{3}MLCT/^{3}LLCT/^{3}ILCT	568 (2.18)
2	$A^3A \rightarrow X^1A$	L → H (0.73)	649 (1.91)	^{3}ILCT	
3	$A^3A \rightarrow X^1A$	L → H (0.70)	661 (1.88)	^{3}MLCT/^{3}LLCT	
4	$A^3A \rightarrow X^1A$	L → H (0.72)	654 (1.90)	^{3}ILCT	

[a] Reference 25.

TABLE 9: Molecular Orbital Compositions (%) of 1−4 in the Lowest-lying Triplet Excited States at the B3LYP Level

orbital	energy (eV)	Ir	N^N	C^N	main bond type	Ir components
1						
L	−3.11		93.4		π^*(N^N)	
H−1	−6.44	20.5	64.9	14.6	d(Ir) + π(N^N) + π(C^N)	10.7 d_{yz} 9.5 d_{xz}
2						
L	−2.59		93.6		π^*(N^N)	
H	−5.43		97.9		π(N^N)	
3						
L	−3.14		93.0		π^*(N^N)	
H	−5.73	41.2		53.5	d(Ir) + π(C^N)	25.1 d_{xz} 5.3 d_{yz} 11.3 d_{z^2} 9.0 $d_{x^2-y^2}$
4						
L	−2.52		93.6		π^*(N^N)	
H	−5.34		98.0		π(N^N)	

increased by 5.4° and 5.8°, but those of **2** and **4** are hardly changed in the excited states by addition of F^- and CH_3COO^-. Other bond angles of **1**−**4** are hardly affected by the excitation. The dihedral angle N5−H−O1−C6 of **4** is increased to 179.8°, which means the backbone of CH_3COO^- and phenanthroline are more coplanar in the excited state than in the ground state. The variations trends of geometry parameters of **3a** from ground to excited states are similar to these of **3**.

By comparing the ground and the excited states geometries of **1**−**4** and **3a**, we found the geometric variations of **1** are similar to those of **3/3a**, and those of **2** have the similar changing trend to those of **4**, which indicated that **1** and **3/3a**, **2** and **4** may have similar spectroscopic properties, and it has been confirmed by the following spectra discussions.

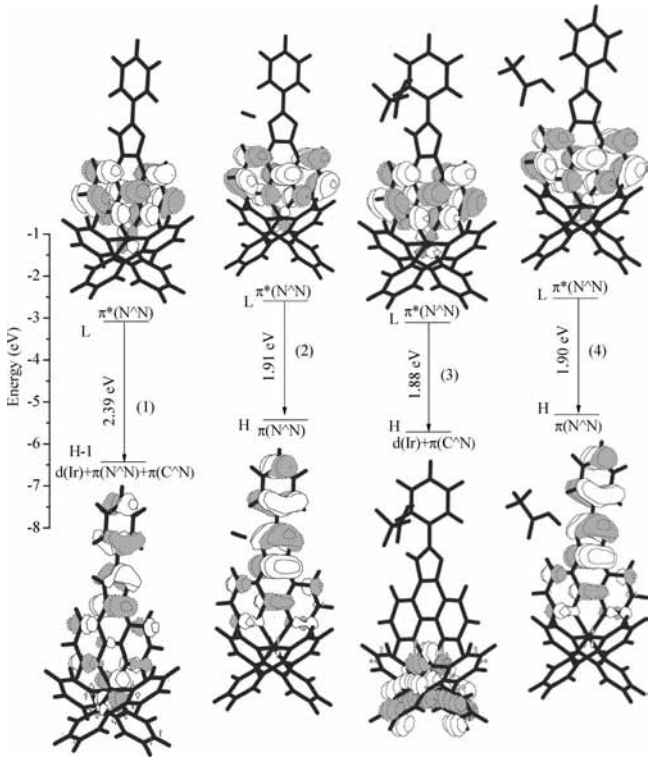

Figure 5. Transitions responsible for the emission at 519, 649, 661, and 654 nm for **1**, **2**, **3**, and **4**, respectively.

NBO Charge Population Analysis. Natural bond orbital (NBO) analysis was also carried out at the same calculation level as the geometry optimization. The calculation results showed that there are −0.72, −0.01, and −0.82 charges on F^-, CF_3COOH, and CH_3COO^- groups, respectively, moreover, there are 0.47, 0.51, 0.44, and 0.47 charges on H atom of N5−H for **1**, **2**, **3**, and **4**, respectively. It is indicated that there is weak interaction between the CF_3COOH and N^N ligand without charge transfer between them, but there is remarkable interaction between the N^N ligand and F^-, CH_3COO^- groups, because there are −0.21 and −0.35 net charges on the $H^+ \cdot F^-$ and $H^+ \cdot CH_3COO^-$ parts. Comparing within $H^+ \cdot F^-$ and $H^+ \cdot CH_3COO^-$, the interaction between H^+ and F^- is stronger than that between H^+ and CH_3COO^-, because the net charge of $H^+ \cdot F^-$ is smaller than that of $H^+ \cdot CH_3COO^-$, so the interaction between $H^+ \cdot F^-$ and N^N ligand is smaller than that between the $H^+ \cdot CH_3COO^-$ and N^N ligand, which is also consistent with the geometry variations by addition of F^- and CH_3COO^- groups. Table 1 shows that the N5−H−O1 bond angle of **3** is 172.5°, close to 180.0°, which indicates that H−O1 bond is a hydrogen bond, but the adsorption between the N5−H bond of the imidazolyl group and F^- is a deprotonation process and not a hydrogen-bonding effect like CF_3COOH, which is consistent with the conclusion obtained by Li and Huang.[25] The calculation results also showed that the interaction between CF_3COOH and N^N of **3a** is similar to that of **3**.

On experiment, Li and Huang[25] reported that **1** can be used as a selective chemosensor for F^- because the binding constants (K) of **1** for F^- (7.01×10) is higher than that of CH_3COO^- (1.42×10^4), and it is consistent with our calculated results that the interaction between H^+ and F^- is stronger than that between H^+ and CH_3COO^-.

Frontier Molecular Orbital Properties. The frontier molecular orbital (FMO) compositions (population analysis using the SCF density) of **1**−**4** are given in Tables 2–5. The calculated results showed that LUMO of **1**, **2**, **3a**, and **4** dominantly contributed by 90.0% π^*(N^N) are hardly affected by the

addition of F^-, CF_3COOH (addition on N6 site) and CH_3COO^-, but the LUMO of **3** composed of 21.8% π*(N^N) and 77.1% π*(CF_3COOH) is greatly changed by addition of CF_3COOH on N5−H site compared with the LUMO of **1**. The LUMO+1 of **1**, **3a**, and **4** are dominantly localized on N^N ligand, that of **2** is contributed by 78.4% π*(N^N) and 19.6% π*(C^N), and that of **3** is composed of 74.8% π*(N^N) and 20.8% π*(CF_3COOH). The HOMOs of **1**−**4** have more than 43.5% d(Ir) and 50.0% π*(C^N). HOMO−1s of **1** and **3/3a** are composed of d(Ir), π(N^N), and π(C^N), but those of **2** and **4** are dominantly localized on N^N ligand.

Table 6 shows that our calculated energy levels of HOMO and LUMO of **1** (in gas phase) are −7.76 and −5.04 eV, which is exactly consistent with the calculated results obtained by Li and Huang[25] with DFT method (HOMO −7.71 eV, LUMO −4.84 eV). In CH_2Cl_2 solvent, the energies of HOMO and LUMO of **1** are greatly increased to −5.86 and −2.83 eV, and these of **3/3a** have similar changing trends to **1**, but with respect to **2** and **4**, the solvent effect is not obvious.

Absorptions in CH_2Cl_2 Media. The calculated absorptions of **1**−**4** associated with their oscillator strengths, the main configurations, and their assignments as well as the experimental results[25] of **1** are given in Table 7. The fitted Gaussian type absorption curves of **1**−**4** are shown in Figure 2. To intuitively understand the transition process, the energy levels of molecular orbital involved in transitions of **1**−**4** are displayed in Figure 3 and the lowest-lying absorption transition diagram of **1**−**4** are shown in Figure 4.

Table 7 and Figure 2 show that the lowest lying distinguishable absorption bands of **1**−**4** are at 412 nm (3.01 eV), 448 nm (2.77 eV), 409 nm (3.03 eV), and 427 nm (2.91 eV), respectively. Table 2 and Figure 3 show that two excitations of H-1 → L and H-3 → L with the configuration coefficients of 0.57 and 0.32 should be responsible for the absorption band at 412 nm of **1**. Table 2 shows that H−1 is composed of 9.5% d_{xy}(Ir), 10.8% d_{yz}(Ir), 60.2% π(N^N), and 19.4% π(C^N), H−3 has 31.9% d_{xz}(Ir), 22.9% d_{z^2}(Ir), and 37.6% π(C^N), whereas the LUMO is dominantly localized on N^N ligand with 94.3% composition. Thus, the lowest-lying absorption at 412 nm of **1** can be assigned to {[d_{yz,xz,xy,z^2}(Ir) + π(N^N) + π(C^N)] → [π*(N^N)]} transition with mixing MLCT/LLCT/ILCT transition characters (See Figure 4). On experiment, the lowest-lying absorption of **1** at 416 is also attributed to MLCT, which is exactly consistent with our calculated results.[25] Figure 4 shows that the lowest-energy absorption at 427 nm of **3** is contributed by {[d_{xy}(Ir) + π(N^N) + π(C^N)] → [π*(N^N)]} with MLCT/LLCT/ILCT transition characters, which is similar to the lowest-energy absorption character of **1**. The lowest-lying absorptions of **2** (448 nm) and **4** (427 nm) have different transition characters from that of **1** and **3**. Tables 3 and 5 show that the LUMO and HOMO of **2** and **4** are dominantly localized on N^N ligand, thus, the lowest-lying absorptions of **2** and **4** are attributed to pure ILCT within N^N ligand, but without MLCT transition characters (see Figure 4). The calculated results showed that the F^-, CH_3COO^- and CF_3COOH groups hardly have contribution to the lowest-lying absorption. Our calculation results also showed that the lowest-lying absroption at 419 nm of **3a** contributed by H−1 → L (0.65) can be described as MLCT/LLCT transition similar to that of **3**, which indicates that the excitation energy and the character of the lowest-lying absorption can not be changed remarkably by different addition sites (N5−H (**3**) and N6 (**3a**)) of CF_3COOH group on N^N ligand.

Figure 3 and Table 7 show that the second and the third distiguishable absorption bands at 351 and 304 nm of **1** contributed by H−2 → L+1 (0.58) and H−2 → L+4 (0.52) excitations, respectively, can be assigned to LLCT/ILCT transitions. The highest energy and strongest absorption band at 280 nm of **1** is contributed by two excitations of H−7 → L+1 (0.40) and H−8 → L+1 (0.40). Table 2 shows that H−7, H−8, and L+1 are all localized on the N^N ligand; thus, this absorption can be described as pure ILCT transition. On experiment, the intense absorption bands below 370 nm of **1** are assigned to spin-allowed IL (π→π*) (ppy and phenanthroline) transition, and the absorption bands at 348 nm, 299 nm, and 279 nm are exactly consistent with our calculated results (see Table 7).[25]

With respect to **2**, the second absorption band at 371 nm contributed by H−2 → L (0.63) excitation is assigned to MLCT/LLCT transition, and the third absorption band at 330 nm is attributed to LLCT/ILCT transition, the strongest and the highest-energy absorption at about 280 nm is contributed by two excitations of $X^1A \rightarrow D^1A$ and $X^1A \rightarrow E^1A$ (X: ground state; A/B/C/D/E: the first/second/third/fourth/fifth excited states), and it is dominantly assigned to ILCT mixed with some MLCT transition character. For **4**, the second lowest-lying absorption band at 364 nm contributed by H−1 → L+1 (0.63) has pure ILCT transition character, the absorption at 323 nm has similar transition character with that at 330 nm of **2**, and the highest-energy absorption band at 273 nm has similar MLCT/ILCT transition character to that at 280 nm of **2**. With respect to **3**, the second absorption band at around 350 nm is contributed by two excitations of $X^1A \rightarrow B^1B$ and $X^1A \rightarrow C^1B$ with mixing MLCT/LLCT transition character. The highest-energy absorption band at 277 nm has the similar ILCT character to the lowest-lying absorption band at 412 nm of **1**. Moreover, the excitation energy and the character of the absorptions of **3a** are similar to these of **3**.

Emission in CH_2Cl_2 Media. The calculated phosphorescence of **1**−**4** in CH_2Cl_2 media together with the measured value[25] of **1** are given in Table 8; the frontier molecular orbital compositions responsible for the emissions are complied in Table 9. To intuitively understand the transition process, the calculated lowest-lying emission transition diagrams of **1**−**4** are showed in Figure 5.

The calculated phosphorescence at 519 nm (2.39 eV) of **1** agrees with the experimental values[25] at 568 nm (2.18 eV) with a deviation of 0.21 eV. The transition of L → H−1 with the configuration coefficient of 0.68 is responsible for the calculated emission at 519 nm. Table 9 shows that LUMO is dominantly contributed by π*(N^N) with 93.4% composition, whereas HOMO−1 is composed of 10.7% d_{yz}(Ir), 9.5% d_{xz}(Ir), 64.9% π(N^N), and 14.6% π(C^N). Thus, the calculated emission at 519 nm can be described as originating from the ^{3}{[$d_{yz,xz}$(Ir) + π(N^N) + π(C^N)] [π*(N^N)]} excited state with ^{3}MLCT/^{3}ILCT/^{3}LLCT characters involving about 20.5% ^{3}MLCT (see Figure 5). With respect to **2** and **4**, Table 9 shows that the HOMO and LUMO are dominantly localized on N^N ligand with more than 93.0% compositions, thus the lowest-energy triplet excited state contributed by L → H transition can be described as ^{3}ILCT characters without ^{3}MLCT compositions (see Figure 5). For **3**, Table 9 shows that HOMO is composed of 25.1% d_{xz}(Ir), 5.3% d_{yz}(Ir), 11.3% d_{z^2}(Ir), 9.0% $d_{x^2-y^2}$(Ir), and 53.5% π(C^N), LUMO is dominantly localized on N^N ligand, thus the calculated phosphorescence at 661 nm contributed by the transition of L → H (0.70) can be described as originating from ^{3}{[d_{xz,yz,z^2,x^2-y^2}(Ir) + π(C^N)] [π*(N^N)]} excited state with ^{3}MLCT/^{3}LLCT characters involving about 41.2% ^{3}MLCT composition. For **3a**, the character of lowest-energy triplet excited state is similar to that of **3**, and the

calculated phosphorescence at 702 nm is also red-shifted compared with that of **1** at 519 nm.

On the investigation of Ru, Os, and Ir complexes, Angelis,[33] Chou and Chi[34] have concluded that the intersystem crossing can be enhanced by notable ^{3}MLCT participation, namely, the phosphorescence ($T_1 \rightarrow S_0$ radiative transition) originating from $^3\pi\pi^*$ mixed with ^{3}MLCT excited states should be greatly increased by increasing the ratio of ^{3}MLCT: $^3\pi\pi^*$. On the theoretical study, Kim[35] found that the phosphorescent complexes will have a high phosphorescent emitting property if the composition of d orbital is large.

On experiment, upon addition of CF_3COOH, the emission wavelength was significantly red-shifted and the emission color changed from yellow to red,[25] which is consistent with our calculated results that the emission of **3/3a** (661/702 nm) is red-shifted compared with that of **1** (519 nm), and the reason for the emissive property of **3/3a** is that the lowest-energy triplet excited state has the emissive ^{3}MLCT character. Li and Huang reported that the emission of **1** was quenched completely upon addition of F^- and CH_3COO^-, which can be interpreted by our calculated results.[25] With respect to our calculated results, the lowest-energy excited state of **2** and **4** have pure ^{3}ILCT character but without the important emissive ^{3}MLCT character, thus, **2** and **4** have no phosphorescence experimentally.

On experiment, the following formulas exist among k_r (radiative decay rate), k_{nr} (nonradiative decay rate), Φ (quantum yield), and τ (lifetime). $k_r = \Phi/\tau$, $k_{nr} = (1 - \Phi)/\tau$, and Φ can be affected by the competition between k_r and k_{nr}, namely, $\Phi = k_r/(k_r + k_{nr})$. So, to increase the quantum yield, k_r should be increased and k_{nr} should be decreased simultaneously or respectively.[33,36] With respect to **2** and **4**, after that addition of F^- and CH_3COO^- anions, there is no ^{3}MLCT character, the K_r is sharply decreased compared with k_{nr}, thus Φ is decreased at the same time, so the phosphorescence of **2** and **4** is quenched, which can be observed by naked eyes. On the other hand, the quantum yield of **3/3a** may be larger than that of **1**, because of the larger ^{3}MLCT composition of **3/3a** (41.2%/40.7%) compared with that of **1** (20.5%) in the triplet excited state.

Conclusions

The present work investigated the ground and excited states geometries, charge population, spectroscopic properties, excited states characters of **1**−**4** and **3a** theoretically. The HOMO can be hardly changed by addition of any addition groups including F^-, CF_3COOH, or CH_3COO^-, but the LUMO can be greatly changed after addition of CF_3COOH. The lowest-lying absorption of **1** and **3/3a** are assigned to MLCT/LLCT/ILCT transition, whereas the lowest-lying absorption of **2** and **4** are attributed to pure ILCT transition. Compared with the phosphorescence of **1**, the phosphorescence of **3/3a** are red-shifted upon addition of CF_3COOH, but the phosphorescence of **2** and **4** are quenched completely upon addition of F^- and CH_3COO^-, the calculated results showed that the ^{3}MLCT character plays an important role in phosphorescence process. Among F^-, CH_3COO^-, and CF_3COOH, F^- has the strongest interaction with H (N5−H), so complex **1** is suitable for the sensor of F^-. It is very practical to explore the relationship between the excited states and the phosphorescence of the Ir(III) complexes sensor. We hope these theoretical studies can provide suggestion in discovering new efficient transition-metal sensors.

Acknowledgment. This work was supported by the Natural Science Foundation of China (Grant Nos. 20573042, 20703015, and 20333050).

References and Notes

(1) (a) Balzani, V.; Juris, A.; Venturi, M.; Campagna, S.; Serroni, S. *Chem. Rev.* **1996**, *96*, 759. (b) Vlček, A., Jr. *Coord. Chem. Rev.* **1998**, *177*, 219. (c) Demadis, K. D.; Hartshorn, C. M.; Meyer, T. J. *Chem. Rev.* **2001**, *101*, 2655. (d) Carlson, B.; Phelan, G. D.; Kaminsky, W.; Dalton, L.; Jiang, X.; Liu, S.; Jen, A. K. Y. *J. Am. Chem. Soc.* **2002**, *124*, 14162. (e) Amarante, D.; Cherian, C.; Catapano, A.; Adams, R.; Wang, M. H.; Megehee, E. G. *Inorg. Chem.* **2005**, *44*, 8804. (f) Tung, Y. L.; Chen, L. S.; Chi, Y.; Chou, P. T.; Cheng, Y. M.; Li, E. Y.; Lee, G. H.; Shu, C. F.; Wu, F. I.; Carty, A. J. *Adv. Funct. Mater.* **2006**, *16*, 1615. (g) Wong, C. Y.; Chan, M. C. W.; Zhu, N. Y.; Che, C. M. *Organometallics* **2004**, *23*, 2263. (h) Lai, S. W.; Lam, H. W.; Lu, W.; Cheung, K. K.; Che, C. M. *Organometallics* **2002**, *21*, 226. (i) Tocher, D. A.; Pal, P. K.; Datta, D. *J. Phys. Chem. A* **2003**, *42*, 7704. (j) Pal, P. K.; Drew, M. G. B.; Datta, D. *New. J. Chem.* **2002**, *26*, 24.

(2) (a) Wand, Y.; Herron, N.; Grushin, V. V.; LeCloux, D. D.; Petrov, V. A. *Appl. Phys. Lett.* **2001**, *79*, 449. (b) Xin, H.; Li, F. Y.; Shi, M.; Bian, Z. Q.; Huang, H. Ch. *J. Am. Chem. Soc.* **2003**, *125*, 7166. (c) Tsuboyama, A.; Iwawaki, H.; Furugori, M.; Mukaide, T.; Kamatani, J.; Igawa, S.; Moriyama, T.; Miura, S.; Takiguchi, T.; Okada, S.; Hoshino, M.; Ueno, K. *J. Am. Chem. Soc.* **2003**, *125*, 12971. (d) Tsuzuki, T.; Tokito, S. *Adv. Mater.* **2007**, *19*, 276. (e) Kwok, C. C.; Ngai, H. M. Y.; Chan, S. C.; Sham, I. H. T.; Che, C. M.; Zhu, N. Y. *Inorg. Chem.* **2005**, *44*, 4442. (f) Che, C. M.; Chan, S. C.; Xiang, H. F.; Chan, M. C. W.; Liu, Y.; Wang, Y. *Chem. Commun.* **2004**, 1484. (g) Yip, W. P.; Ho, C. M.; Zhu, N. Y.; Lau, T. C.; Che, C. M. *Chem. Asian J.* **2008**, *3*, 70.

(3) (a) Lo, K. K. W.; Chung, C. K.; Lee, T. K. M.; Lui, L. H.; Tsang, K. H. K.; Zhu, N. Y. *Inorg. Chem.* **2003**, *42*, 6886. (b) Lo, K. K. W.; Ng, D. C. M.; Chung, C. K. *Organometallics* **2001**, *20*, 4999.

(4) (a) Haynes, A.; Maitlis, P. M.; Morris, G. E.; Sunley, G. J.; Adams, H.; Badger, P. W.; Bowers, C. M.; Cook, D. B.; Elliott, P. I. P.; Ghaffar, T.; Green, H.; Griffin, T. R.; Payne, M.; Pearson, J. M.; Taylor, M. J.; Vickers, P. W.; Watt, R. J. *J. Am. Chem. Soc.* **2004**, *126*, 2847. (b) Oxgaard, J.; Bhalla, G.; Periana, R. A.; Goddard, W. A., III. *Organometallics* **2006**, *25*, 1618. (c) McKinney, R. J.; Colton, M. C. *Organometallics* **1986**, *5*, 1080. (d) Pertici, P.; Ballantini, V.; Salvadori, P.; Bennett, M. A. *Organometallics* **1995**, *14*, 2565. (e) Silaware, N. D.; Goldman, A. S.; Ritter, R.; Tyler, D. R. *Inorg. Chem.* **1989**, *28*, 1231.

(5) (a) Bondy, C. R.; Loeb, S. J. *Coord. Chem. Rev.* **2003**, *240*, 77. (b) Beer, P. D.; Hayes, E. J. *Coord. Chem. Rev.* **2003**, *240*, 167. (c) Xu, G. X.; Tarr, M. A. *Chem. Commun.* **2004**, *1050.* (d) Suksai, C.; Tuntulani, T. *Chem. Soc. Rev.* **2003**, *32*, 192. (e) Bühlmann, P.; Pretsch, E.; Bakker, E. *Chem. Rev.* **1998**, *98*, 1593. (f) Cho, E. J.; Moon, J. W.; Ko, S. W.; Lee, J. Y.; Kim, S. K.; Yoon, J.; Nam, K. C. *J. Am. Chem. Soc.* **2003**, *125*, 12376. (g) Ghosh, T.; Maiya, B. G.; Wong, M. W. *J. Phys. Chem. A* **2004**, *108*, 11249.

(6) (a) de Silva, A. P.; Gunaratne, H. Q. N.; Gunnlaugsson, T.; Huxley, A. J. M.; McCoy, C. P.; Rademacher, J. T.; Rice, T. E. *Chem. Rev.* **1997**, *97*, 1515. (b) Demas, J. N.; DeGraff, B. A. *Coord. Chem. Rev.* **2001**, *211*, 317.

(7) Carraway, E. R.; Demas, J. N.; DeGraff, B. A.; Bacon, J. R. *Anal. Chem.* **1991**, *63*, 337.

(8) Di Marco, G.; Lanza, M.; Mamo, A.; Stefio, I.; Di Pietro, C.; Romeo, G.; Campagna, S. *Anal. Chem.* **1998**, *70*, 5019.

(9) Zhao, Y. G.; Lin, Z. H.; Ou, S. J.; Duan, C. Y.; Liao, H. P.; Bai, Z. P. *Inorg. Chem. Commun.* **2006**, *9*, 802.

(10) Ghosh, A.; Ganguly, B.; Das, A. *Inorg. Chem.* **2001**, *40*, 5507.

(11) McGee, K. A.; Veltkamp, D. J.; Marquardt, B. J.; Mann, K. R. *J. Am. Chem. Soc.* **2007**, *129*, 15092.

(12) Lam, M. H. W.; Lee, D. Y. K.; Man, K. W.; Lau, C. S. W. *J. Mater. Chem.* **2000**, *10*, 1825.

(13) Huynh, L.; Wang, Z.; Yang, J.; Stoeva, V.; Lough, A.; Manners, I.; Winnik, M. A. *Chem. Mater.* **2005**, *17*, 4765.

(14) (a) Wong, K. M. C.; Tang, W. S.; Lu, X. X.; Zhu, N. Y.; Yam, V. W. W. *Inorg. Chem.* **2005**, *44*, 1492. (b) Tang, W. S.; Lu, X. X.; Wong, K. M C.; Yam, X. W. W. *J. Mater. Chem.* **2005**, *15*, 2714.

(15) (a) Lamansky, S.; Djurovich, P.; Murphy, D.; Abdel−Razzaq, F.; Lee, H. E.; Adachi, C.; Burrows, P. E.; Forrest, S. R.; Thompson, M. E. *J. Am. Chem. Soc.* **2001**, *123*, 4304. (b) Lamansky, S.; Djurovich, P.; Murphy, D.; Abdel−Razzaq, F.; Kwong, R.; Tsyba, I.; Bortz, M.; Mui, B.; Bau, R.; Thompson, M. E. *Inorg. Chem.* **2001**, *40*, 1704.

(16) Hay, P. J. *J. Phys. Chem. A* **2002**, *106*, 1634.

(17) (a) Markham, J. P. J.; Lo, S. C.; Magennis, S. W.; Burn, P. L.; Samuel, I. D. W. *Appl. Phys. Lett.* **2002**, *80*, 2645. (b) Colombo, M. G.; Gudel, H. U. *Inorg. Chem.* **1993**, *32*, 3081. (c) Baldo, M. A.; Lamansky, S.; Burrows, P. E.; Thompson, M. E.; Forrest, S. R. *Appl. Phys. Lett.* **1999**, *75*, 4.

(18) (a) Ostrowski, J. C.; Robinson, M. R.; Heeger, A. J.; Bazan, G. C. *Chem. Commun.* **2002**, 784. (b) Yang, C. H.; Cheng, Y. M.; Chi, Y.; Hsu, C. J.; Fang, F. C.; Wong, K. T.; Chou, P. T.; Chang, C. H.; Tsai, M. H.; Wu, C. C. *Angew. Chem., Int. Ed.* **2007**, *46*, 2418. (c) Yang, C. H.; Tai, C. C.; Sun, I. W. *J. Mater. Chem.* **2004**, *14*, 947. (d) Wong, W. Y.; Ho,

C. L.; Gao, Z. Q.; Mi, B. X.; Chen, C. H.; Cheah, K. W.; Lin, Z. Y. *Angew. Chem., Int. Ed.* **2006**, *45*, 7800. (e) Wong, W. Y.; Zhou, G. J.; Yu, X. M.; Kwok, H. S.; Lin, Z. Y. *Adv. Funct. Mater.* **2007**, *17*, 315. (f) Wong, W. Y.; Zhou, G. J.; Yu, X. M.; Kwok, H. S.; Tang, B. Z. *Adv. Funct. Mater.* **2006**, *16*, 838. (g) Zhou, G. J.; Wong, W. Y.; Yao, B.; Xie, Z. Y.; Wang, L. X. *Angew. Chem., Int. Ed.* **2007**, *46*, 1149. (h) Zhou, G. J.; Wong, W. Y.; Yao, B.; Xie, Z. Y.; Wang, L. X. *J. Mater. Chem.* **2008**, *18*, 1799. (i) Ho, C. L.; Wong, W. L.; Wang, Q.; Ma, D. G.; Wang, L. X.; Lin, Z. Y. *Adv. Funct. Mater.* **2008**, *18*, 928. (j) Zhou, G. J.; Ho, C. L.; Wong, W. Y.; Wang, Q.; Ma, D. G.; Wang, L. X.; Lin, Z. Y.; Marder, T. B.; Beeby, A. *Adv. Funct. Mater.* **2008**, *18*, 499. (k) Ho, C. L.; Wong, W. Y.; Gao, Z. Q.; Chen, C. H.; Cheah, K. W.; Yao, B.; Xie, Z. Y.; Wang, Q.; Ma, D. G.; Wang, L. X.; Yu, X. M.; Kwok, H. S.; Lin, Z. Y. *Adv. Funct. Mater.* **2008**, *18*, 319.

(19) (a) Gao, R.; Ho, D. G.; Hernandez, B.; Selke, M.; Murphy, D.; Djurovich, P. L.; Thompson, M. E. *J. Am. Chem. Soc.* **2002**, *124*, 14828. (b) Borisov, S. M.; Klimant, I. *Anal. Chem.* **2007**, *79*, 7501.

(20) Chen, H. L.; Zhao, Q.; Wu, Y. B.; Li, F. Y.; Yang, H.; Yi, T.; Huang, C. H. *Inorg. Chem.* **2007**, *46*, 11075.

(21) Zhao, Q.; Cao, T. Y.; Li, F. Y.; Li, X. H.; Jing, H.; Yi, T.; Huang, C. H. *Organometallics* **2007**, *26*, 2077.

(22) Schmittel, M.; Lin, H. W. *Inorg. Chem.* **2007**, *46*, 9139.

(23) Goodall, W.; Williams, J. A. G. *J. Chem. Soc., Dalton Trans.* **2000**, *2893*.

(24) (a) Lo, K. K. W.; Chan, J. S. W.; Lui, L. H.; Chung, C. K. *Organometallics* **2004**, *23*, 3108. (b) Lo, K. K. W.; Hui, W. K.; Chung, C. K.; Tsang, K. H. K.; Ng, D. C. M.; Zhu, N. Y.; Cheung, K. K. *Coord. Chem. Rev.* **2005**, *249*, 1434. (c) Lo, K. K. W.; Hui, W. K.; Chung, C. K.; Tsang, K. H. K.; Lee, T. K. M.; Li, C. K.; Lau, J. S. Y.; Ng, D. C. M. *Coord. Chem. Rev.* **2006**, *250*, 1724. (d) Lo, K. K. W.; Lau, J. S. Y.; Lo, D. K. K.; Lo, L. T. L. *Eur. J. Inorg. Chem.* **2006**, 4054. (e) Lo, K. K. W.; Lau, J. S. Y. *Inorg. Chem.* **2007**, *46*, 700.

(25) Zhao, Q.; Liu, S. J.; Shi, M.; Li, F. Y.; Jing, H.; Yi, T.; Huang, C. H. *Organometallics* **2007**, *26*, 5922.

(26) Runge, E.; Gross, E. K. U. *Phys. Rev. Lett.* **1984**, *52*, 997.

(27) Becke, A. D. *J. Chem. Phys.* **1993**, *98*, 5648.

(28) (a) Stratmann, R. E.; Scuseria, G. E. *J. Chem. Phys.* **1998**, *109*, 8218. (b) Matsuzawa, N. N.; Ishitani, A. *J. Phys. Chem. A* **2001**, *105*, 4953. (c) Casida, M. E.; Jamorski, C.; Casida, K. C.; Salahub, D. R. *J. Chem. Phys.* **1998**, *108*, 4439.

(29) (a) Cossi, M.; Scalmani, G.; Regar, N.; Barone, V. *J. Chem. Phys.* **2002**, *117*, 43. (b) Barone, V.; Cossi, M. *J. Chem. Phys.* **1997**, *107*, 3210.

(30) (a) Liu, T.; Zhang, H. X.; Xia, B. H. *J. Phys. Chem. A* **2007**, *111*, 8724. (b) Li, J.; Xu, L. C.; Chen, J. C.; Zheng, K. C.; Ji, L. N. *J. Phys. Chem. A* **2006**, *110*, 8174. (c) Zheng, K. C.; Wang, J. P.; Peng, W. L.; Liu, X. W.; Yun, F. C. *J. Mol. Struct. (THEOCHEM)* **2005**, *717*, 179. (d) Li, J.; Chen, J. C.; Xu, L. C.; Zheng, K. C.; Ji, L. N. *J. Organomet. Chem.* **2007**, *692*, 831.

(31) (a) Hay, P. J.; Wadt, W. R. *J. Chem. Phys.* **1985**, *82*, 299. (b) Hay, P. J.; Wadt, W. R. *J. Chem. Phys.* **1985**, *82*, 270.

(32) Frisch, M. J.; Trucks, G. W.; Schlegel, H. B.; Scuseria, G. E.; Robb, M. A.; Cheeseman, J. R.; Montgomery, J. A., Jr.; Vreven, T.; Kudin, K. N.; Burant, J. C.; Millam, J. M.; Iyengar, S. S.; Tomasi, J.; Barone, V.; Mennucci, B.; Cossi, M.; Scalmani, G.; Rega, N.; Petersson, G. A.; Nakatsuji, H.; Hada, M.; Ehara, M.; Toyota, K.; Fukuda, R.; Hasegawa, J.; Ishida, M.; Nakajima, T.; Honda, Y.; Kitao, O.; Nakai, H.; Klene, M.; Li, X.; Knox, J. E.; Hratchian, H. P.; Cross, J. B.; Adamo, C.; Jaramillo, J.; Gomperts, R.; Stratmann, R. E.; Yazyev, O.; Austin, A. J.; Cammi, R.; Pomelli, C.; Ochterski, J. W.; Ayala, P. Y.; Morokuma, K.; Voth, G. A.; Salvador, P.; Dannenberg, J. J.; Zakrzewski, V. G.; Dapprich, S.; Daniels, A. D.; Strain, M. C.; Farkas, O.; Malick, D. K.; Rabuck, A. D.; Raghavachari, K.; Foresman, J. B.; Ortiz, J. V.; Cui, Q.; Baboul, A. G.; Clifford, S.; Cioslowski, J.; Stefanov, B. B.; Liu, G.; Liashenko, A.; Piskorz, P.; Komaromi, I.; Martin, R. L.; Fox, D. J.; Keith, T.; Al-Laham, M. A.; Peng, C. Y.; Nanayakkara, A.; Challacombe, M.; Gill, P. M. W.; Johnson, B.; Chen, W.; Wong, M. W.; Gonzalez, C.; Pople, J. A. *Gaussian 03*, revision C.02; Gaussian, Inc.: Wallingford, CT, 2004.

(33) (a) De Angelis, F.; Fantacci, S.; Evans, N.; Klein, C.; Zakeeruddin, S. M.; Moser, J. E.; Kalyanasundaram, K.; Bolink, H. J.; Grätzel, M.; Nazeeruddin, M. K. *Inorg. Chem.* **2007**, *46*, 5989. (b) Fantacci, S.; De Angelis, F.; Sgamellotti, S.; Marrone, A.; Re, N. *J. Am. Chem. Soc.* **2005**, *127*, 14144.

(34) (a) Chou, P. T.; Chi, Y. *Chem. Eur. J.* **2007**, *13*, 380. (b) Chi, Y.; Chou, P. T. *Chem. Soc. Rev.* **2007**, *36*, 1421. (c) Li, E. Y.; Cheng, Y. M.; Hsu, C. C.; Chou, P. T.; Lee, G. H.; Lin, I. H.; Chi, Y.; Liu, C. S. *Inorg. Chem.* **2006**, *45*, 8041.

(35) (a) Kim, Y. S.; Kim, H. L. *Curr. Appl. Phys.* **2007**, *7*, 504. (b) Kim, Y. S.; Young, H. L. *Thin Solid Films* **2007**, *515*, 5079.

(36) (a) Lo, S. C.; Shipley, C. P.; Bera, R. N.; Harding, R. E.; Cowley, A. R.; Burn, P. L.; Samuel, I. D. W. *Chem. Mater.* **2006**, *18*, 5119. (b) Yang, C. H.; Li, S. W.; Chi, Y.; Cheng, Y. M.; Yeh, Y. S.; Chou, P. T.; Lee, G. H.; Wang, C. H.; Shu, C. F. *Inorg. Chem.* **2005**, *44*, 7770.

JP803996Y